Active Thermal Control via Power Routing of Parallel Inverters in All-Electric Ships

S M Imrat Rahman[1*], Mustafa Ozden[1,2], Gokhan Ozkan[1,2], Ali Moghassemi[1], Laxman Timilsina[1], Okan Ciftci[1], Behnaz Papari[1,3], Zheyu Zhang[4] Christopher S. Edrington[1]
Emails: {smimrar*;mozden;gokhano;amoghas;ltimils;ociftci;bpapari;cedring}@clemson.edu, zhangz49@rpi.edu
[1]*Holcombe Department of Electrical and Computer Engineering, Clemson University, Clemson 29634, SC, USA*
[2]*Dominion Energy Innovation Center, Clemson University, North Charleston 29405, SC, USA*
[3]*Department of Automotive Engineering, Clemson University, Greenville 29607, SC, USA*
[4]*Electrical, Computer, and Systems Engineering, Rensselaer Polytechnic Institute, Troy 12180, NY, USA*

2025 IEEE Electric Ship Technologies Symposium (ESTS) | 979-8-3315-2517-0/25/$31.00 ©2025 IEEE | DOI: 10.1109/ESTS62818.2025.11152420

***Abstract*—The application of power electronics in all-electric ships (AES) has grown significantly because they offer better control and flexibility. Additionally, Induction Motors (IM) are favored in AESs for their reliability, cost-effectiveness and superior speed and torque tracking performance. The reliability of the power converters in AESs is essential for their safe operation, and this is driving interest in new technologies that ensure safe and reliable PEC performance. One major challenge in achieving reliable PEC operation is the efficient management of generated heat. This includes control of junction temperature and regulation of thermal cycles in power semiconductors. Active Thermal Control (ATC) reduces high junction temperature and thermal cycles by using temperature-related control parameters. This paper presents a closed-loop ATC approach via power routing of parallel DC-AC converters that efficiently distributes the thermal load across various segments of a modular converter, thereby minimizing thermal stress on the most vulnerable components. The effectiveness of the proposed thermal management approach is validated through MATLAB/Simulink results.**

***Index Terms*—Active Thermal Control, AES, Electro-Thermal Management, FCS-MPC, Power Routing, Thermal Model, Induction Motor Drive.**

I. Introduction

Power electronic converters (PEC) are utilized across various industries and applications such as electric vehicles (EV) [1], all-electric ship (AES) power systems [2], electrical grids [3], renewable energy-based sources [4], more electric aircraft (MEA) [5] and so on. Power electronics play a critical role in AESs by allowing efficient energy conversion. In recent years, the requirements regarding the reliability of PECs in AESs have been extended to ensure their safe and reliable operation. Research on the reliability of power converters has shown that power semiconductor devices (PSDs) are the most failure-prone components in a PEC, with temperature being the primary cause of their failure [6], [7]. As a result, there is increasing interest in developing effective thermal management systems (TMS) that regulate the degradation rate of power semiconductors by reducing the thermal stress due to over-temperature and power cycling [8]. Active thermal control (ATC) can be employed to regulate the junction temperature of semiconductor devices to minimize temperature-induced failures and enhance system efficiency [9]. Moreover, maintenance of PECs in AESs needs skilled expertise, and system downtime depends on the severity of the failure. Unplanned maintenance can cause disruption in operation, so maintenance scheduling is becoming crucial for ensuring the reliability and availability of PECs. Recently, researchers have focused on optimizing the maintenance schedule by extending the remaining useful life (RUL) of PECs [10]. However, there is little research on actively extending the RUL and optimizing maintenance schedules. This paper presents an ATC approach for optimizing the RUL of PECs through the power routing method. In this method, the power-sharing between converters in a multi-converter system is based on power semiconductor degradation, thus optimizing maintenance, lowering costs and improving efficiency.

A. Power Routing Concept

Power routing is an ATC approach that regulates the distribution of thermal load across different sections of a modular converter, effectively reducing thermal stress on the most vulnerable components and optimizing their remaining useful life (RUL) [11]. By applying this method, each module in a modular configuration of PEC is assigned to handle a specific amount of the total power to reduce thermal stress caused by temperature fluctuations in that module. The objective of this method is to enhance the lifespan of the most deteriorated modules within a modular power converter. This is accomplished by dynamically adjusting their load conditions, thereby minimizing thermal stress on the more degraded modules and redistributing their load to modules that are less degraded. Figure 1a illustrates a modular converter, where each module (1, 2, and 3) carries a portion of the total power, represented as P_1, P_2, and P_3. Under normal conditions, the total power P_T is shared equally among the modules, meaning $P_1 = P_2 = P_3$. However, when power is evenly distributed over time, some

This material is based upon research supported by the US Office of Naval Research (ONR) under award number N00014-22-1-2558, and it is approved for public release under DCN# 2025-2-11-584

modules may wear out faster than others, increasing the risk of unexpected failures and unplanned maintenance. To address this, the power routing technique is used, as shown in Figure 1b. This method adjusts the power each module handles based on its aging condition. By shifting the load between modules, power routing helps reduce stress on older components, allowing for better maintenance planning and extending the overall lifespan of the modular converter.

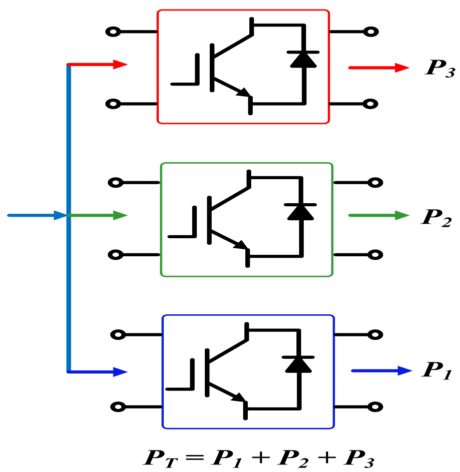

(a) Power routing concept

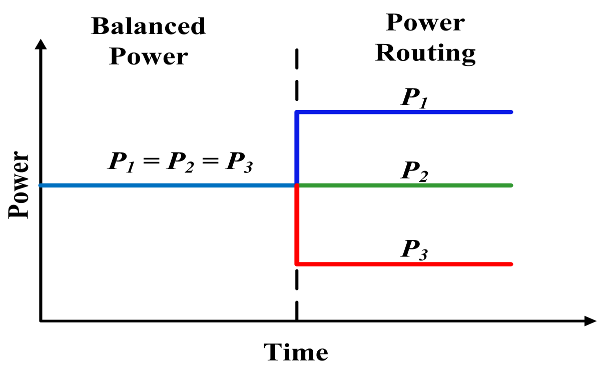

(b) Power balancing between modules

Fig. 1. Power routing in a modular converter system

In a modular converter, the cells can be arranged in series, parallel, or a combination of both [8]. For series connected modules, the power output of each cell is controlled by regulating its output voltage. Similarly, when the modules are parallel connected, the power output is managed by controlling the output current of each cell. In a combined configuration, the power output of each cell can be regulated by adjusting either voltage, current, or both. To use power routing effectively, it is important to estimate the remaining useful life (RUL) and state of health (SOH) of the converters, as explained in [12]. With this information, maintenance can be planned for all modules in the power electronic converter (PEC) based on their individual RUL, ensuring efficient operation and extended lifespan.

B. Contribution of the Paper

The primary contribution of this paper is the development of a comprehensive thermal management framework employing power routing-based ATC for power converters in all-electric ships (AES). This ATC approach enhances the reliability of power converters and optimizes their lifespan. A Cauer-based thermal network is employed to estimate the junction temperature accurately, enabling control algorithm implementation. Simulation results are presented to demonstrate how the junction temperature of PSDs can be regulated based on degradation to optimize the RUL of degraded MOSFETs.

C. Structure of the Paper

The paper is organized as follows. Section II presents related works and the mathematical model of the power routing-based ATC. Section III presents the proposed thermal management scheme. Section IV presents simulation results based on different scenarios. Finally, Section V concludes the paper with suggestions for future work.

II. Electro-Thermal Management with Power Routing Based ATC

A. Literature Review

Several methods have been studied in the literature for implementing power routing techniques for different converter configurations. A closed-loop controller was introduced in [13] to reduce maintenance costs in a parallel-connected three-cell DC-DC converter by considering the state of health (SOH) of each cell. In this control method, an SOH block estimates the degradation level of each cell by analyzing real-time electrical measurements and the system's usage history. The SOH block then sends a reference to the thermal controller, which determines the appropriate power-sharing scheme for the parallel-connected cells. Another study by Marquez et al. [14] introduced a power routing method to reduce aging differences in an interleaved boost converter consisting of three modules. By applying this power routing technique, the study showed that the lifespan of the most degraded power module could be extended by 24 months.

Additional power routing algorithms for more electric aircraft (MEA) with parallel dual active bridges (DAB) are discussed in [15] and [16]. These algorithms aim to extend the overall system lifetime by estimating the remaining useful life (RUL) of the converters. The estimation is based on the junction temperature profiles, which are determined by the mission profile. A study in [17] explored how power routing affects the aging of 10 parallel-connected dual active bridge (DAB) cells in a smart transformer. Another study by Liserre et al. [8] showed that power routing helps reduce thermal cycling effects on the most aged cells in the low-voltage stage of a smart transformer. Additionally, a study in [18] evaluated the effectiveness of a power routing method based on virtual resistors in decreasing thermal stress in a modular converter with multiple quadruple active bridge (QAB) converters. The results showed that the control algorithm helps extend the system's operational lifespan.

Modified modulation strategies allow power routing by controlling thermal stress in each converter. A method called discontinuous PWM (DPWM) for cascaded H-Bridge (CHB) converters is introduced in [19]. DPWM operates by clamping the output voltage to the positive or negative DC-link voltage, preventing unnecessary switching and minimizing losses compared to continuous PWM. This method uses two modulation signals. The first adds a positive offset to the reference voltage, creating a clamping zone, which helps reduce losses in the most vulnerable converters. The second uses a negative offset without a clamping zone and is applied to less vulnerable converters to balance the power distribution. The goal of this strategy is to minimize thermal stress and extend the lifespan of the most affected converters.

A power routing method for STs was proposed in [20], introducing an advanced discontinuous modulation technique to reduce thermal stress in cascaded H-Bridge (CHB) converters and isolated DC/DC converters. Another study in [21] focused on enhancing the thermal performance of CHB converters using a phase-shifted PWM technique, which extends the lifespan of vulnerable cells while reducing harmonic distortion. A different approach, presented in [22], introduced a power routing method based on multi-frequency modulation. This technique injects a third harmonic component into the duty cycle of CHB converters, optimizing DC-link voltage usage similarly to third harmonic injected PWM (THIPWM). These power routing techniques help manage thermal stress more efficiently and improve the overall performance of smart transformers.

B. Virtual Resistance based Power Routing

Andresen et al. [23] proposed a power routing method using virtual resistors for parallel converters in a smart transformer. This method is applied during partial load conditions by adjusting virtual resistors based on condition monitoring data. Optimizing power distribution among the converters improves system performance and extends its operational lifespan. A control method for employing the power routing technique is depicted in Figure 2.

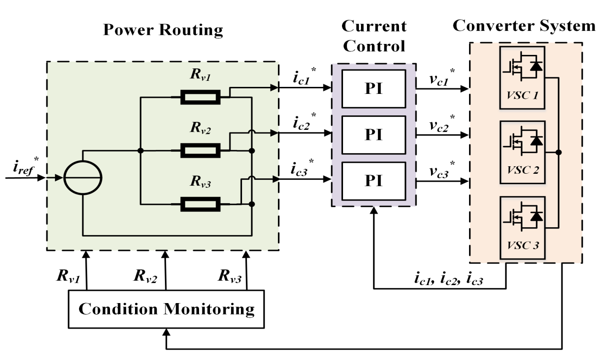

Fig. 2. Virtual resistor-based power routing method

Here, three virtual resistors (R_{v1}, R_{v2}, and R_{v3}) are tuned based on information received from the condition monitor and are expressed as a function of accumulated damage as expressed in (1) [23].

$$R_{vi} = f(D_{acc}) \tag{1}$$

Converter reference currents (i_{cn}^*) can be calculated by using (2).

$$[i_{c1}^*, i_{c2}^*, i_{c3}^*] = \left(\frac{i_{ref}^*}{R_{v2}R_{v3} + R_{v1}R_{v2} + R_{v1}R_{v3}} \right) \cdot [R_{v2}R_{v3}, R_{v1}R_{v2}, R_{v1}R_{v3}] \tag{2}$$

C. Lifetime Estimation

The fluctuations in junction temperature, ΔT_j, and the average junction temperature, T_{avg} influences the life of the power devices. Coffin–Manson's equation(3) provides an estimation of the number of thermal cycles to failure(N_f).

$$N_f = a \cdot (\Delta T_j)^{-n} \cdot e^{\frac{E_a}{k_B \cdot T_m}} \tag{3}$$

Here, N_f is the number of cycles to failure, a represents the experimental coefficient, ΔT_j represents the thermal cycles, n is the experimental coefficient, k_B is the Boltzmann constant, and E_a is the activation energy.

Then the lifetime is estimated according to Miner's rule [24]. The estimate of the accumulated damage is D, calculated using Miner's equation (4):

$$D = \sum_{i=1}^{k} \frac{N_{c,i}}{N_{f,i}} \tag{4}$$

The parameter T indicates how many cycles the device can operate before failure, expressed using (5).

$$T = \frac{1}{D} \tag{5}$$

Here, D is the total damage, $N_{c,i}$ is the number of cycles associated with the i-th operating condition, $N_{f,i}$ is the number of cycles to failure for that specific operating condition, and k is the number of stresses. By calculating $N_{c,i}/N_{f,i}$, the total damage to the MOSFETs can be estimated. Damage lesser than 1 indicates the MOSFET can handle the thermal stresses experienced throughout the operation. For calculating the lifetime, equation (6) can be used [24].

$$\text{Lifetime} = \sum_{t=1}^{k} \frac{1}{3600 \cdot h \cdot 365 \cdot w_t \cdot D_t} \tag{6}$$

Here, h is the number of working hours per day, w_i is the weight factor, D_i is the damage corresponding to the operating condition, and k is the total number of stresses.

D. Degradation Estimation

An increase in the junction-to-case thermal resistance (R_{thjc}) is an indicator of solder fatigue failure [25]. The R_{thjc} exhibits a steady degradation over the component's lifetime and changes gradually while the converter is in operation. In this paper, this behavior of the R_{thjc} is integrated into the thermal model to determine the junction temperature when a MOSFET is degraded. The parameters used for this analysis are presented in Table I [25].

TABLE I
DEVICE DEGRADATION WITH LIFETIME-LEVEL

Lifetime Level (%)	Normalized R_{th_ic}
0–20	1.0
20–40	1.1
40–60	1.2
60–80	1.3
80–100	1.4

Based on the amount of degradation, the control algorithm determines appropriate reference currents for each of the converters to optimize their lifetime and protect the MOSFET from higher degradation.

III. Methodology and Modeling

A. Finite-Control Set Model Predictive Control (FCS-MPC)

Finite Set Model Predictive Control (FS-MPC) enables the development and discretization of mathematical models for drive systems to predict future system variable values within a sampling period using a fixed number of steps. Since an inverter has a limited number of switching states, MPC is implemented by minimizing a cost function for each switching state and selecting the state corresponding to the minimum cost. The cost function is evaluated based on the predicted outcomes, and the optimal prediction is applied for the subsequent calculation. The primary components of this control scheme are the system model and the cost function. The operating principal of FS-MPC is shown in Figure 3.

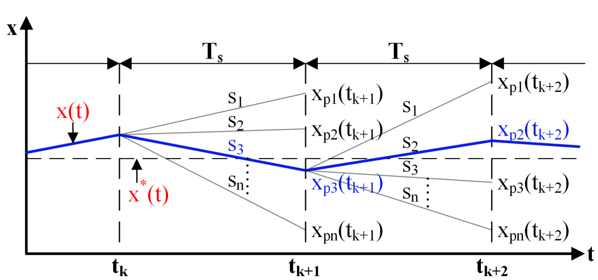

Fig. 3. FS-MPC operating principle

The algorithm of MPC has to calculate an appropriate control action that will enable a system variable to follow a reference value. MPC determines the optimal control action $s(t)$ (e.g., gate signals) to drive a system variable $x(t)$ close to a reference $x^*(t)$. Over each sampling period T_s, the controller predicts possible future states $x_{p_i}(t_{k+1})$ for all control actions s_i $(i = 1, \dots, n)$ using a prediction function f_p. A cost function f_g, typically based on the error $g_i = |x^*(t_{k+1}) - x_{p_i}(t_{k+1})|$, evaluates these predictions. The control action with the minimum cost $(\min\{g_i\})$ is selected and applied.

B. Three-level NPC Model

NPC inverters are widely utilized in medium and high-voltage applications [26]. The voltage stress on the PSDs of a three-level NPC inverter is half compared to a two-level converter. Additionally, NPC inverters offer several advantages, including lower switching losses and reduced harmonic components in the output current waveform. The associated benefits also reduce stress on the motor's windings driven by the inverter. The configuration of the NPC inverter employed in this study is shown in Figure 4.

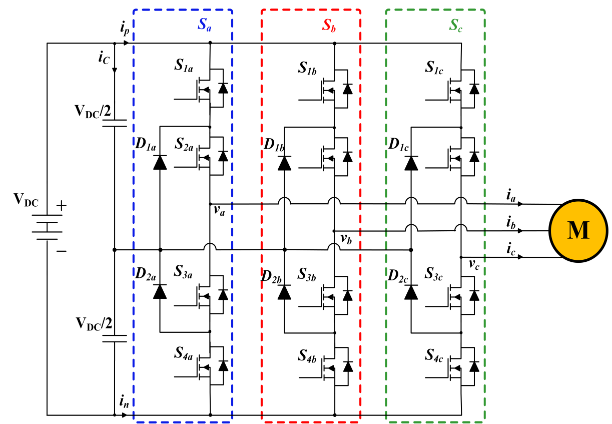

Fig. 4. SiC-based three-level neutral point clamped inverter

Each leg of the NPC inverter comprises four MOSFETs and two clamping diodes. This configuration allows for three valid switching states per leg, resulting in three distinct voltage levels, as shown in Table II.

TABLE II
SWITCHING STATES AND OUTPUT VOLTAGES

S_{1a}	S_{2a}	S_{3a}	S_{4a}	V_{out}	State
ON	ON	OFF	OFF	$V_{DC}/2$	P
OFF	OFF	ON	ON	$-V_{DC}/2$	N
OFF	ON	ON	OFF	0	O

In this paper, a half-bridge SiC-based MOSFET module has been selected as the PSD.

C. Power Loss Calculation

This paper primarily examines the MOSFET losses, specifically focusing on conduction and switching losses. The conduction and switching losses are calculated using equations (7) and (8), respectively [27]. The necessary parameters for calculating these losses are provided in the MOSFET module datasheet.

$$P_{\text{sw}} = (E_{\text{on}} + E_{\text{off}}) \left(\frac{i_D}{i_{\text{ref}}}\right)^{K_i} \left(\frac{v_{\text{dc}}}{v_{\text{ref}}}\right)^{K_v} \cdot (1 + c_{T,\text{sw}}(T_j - T_{j,\text{ref}})) \cdot f_s \tag{7}$$

$$P_{\text{cond}} = R_{\text{DS,on}} \cdot I_D^2 \tag{8}$$

Here, E_{on} and E_{off} are the turn-on and turn-off switching energy, respectively. i_D is the MOSFET drain current. i_{ref}, v_{ref}, and $T_{j,\text{ref}}$ are the current, voltage, and junction temperature reference points, respectively. K_i, K_v, and $c_{T,\text{sw}}$ are empirical constants. f_s is the switching frequency. $R_{\text{DS,on}}$ and I_D are the on-state resistance and drain current, respectively.

D. Thermal Model

In this paper, a thermal model based on the Cauer network is applied because it is suitable for online junction temperature measurement. The Cauer-type network offers the significant advantage of more accurately representing the physical properties of the heat conduction path. Additionally, it allows for independent modeling of the heat sink and semiconductor device. Considering data accuracy and computational burden, the thermal model considered in this study consists of 3 RC cells as depicted in Figure 5.

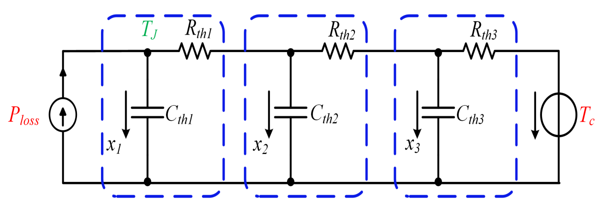

Fig. 5. Developed thermal model

The junction and case temperatures are represented by T_j and T_C, respectively, while the power loss is denoted by P_{loss}.The junction-to-case heat conduction path is represented by three nodes, each comprising an equivalent thermal resistor (R_{th}) and capacitor (C_{th}). The RC parameters have been extracted from the thermal impedance curve using SaberRD software.

The state equations (9-11) for the developed thermal model are derived by applying Kirchhoff's laws.

$$\frac{dx_1}{dt} = -\frac{1}{C_{\text{th1}} R_{\text{th1}}} x_1 + \frac{1}{C_{\text{th1}} R_{\text{th1}}} x_2 + \frac{1}{C_{\text{th1}}} P_{\text{loss}} \tag{9}$$

$$\frac{dx_2}{dt} = \frac{1}{C_{\text{th2}} R_{\text{th1}}} x_1 - \frac{R_{\text{th1}} + R_{\text{th2}}}{C_{\text{th2}} R_{\text{th1}} R_{\text{th2}}} x_2 + \frac{1}{C_{\text{th2}} R_{\text{th2}}} x_3 \tag{10}$$

$$\frac{dx_3}{dt} = \frac{1}{C_{\text{th3}} R_{\text{th2}}} x_2 - \frac{R_{\text{th2}} + R_{\text{th3}}}{C_{\text{th3}} R_{\text{th2}} R_{\text{th3}}} x_3 + \frac{1}{C_{\text{th3}} R_{\text{th3}}} T_C \tag{11}$$

These state equations are utilized to estimate the junction temperature of the MOSFETs for any specific values of power loss and case temperature.

E. Electro-Thermal Management Framework

A comprehensive control framework for a power routing system integrated with predictive control and thermal management has been developed in this work. The framework is illustrated in Figure 6. This framework regulates junction temperature and thermal cycling of power converters using virtual resistance-based power routing and degradation management.

The physical system includes two NPC converters (NPC_1 & NPC_2) connected to an induction machine. The induction motor parameters are listed in Table III.

TABLE III
INDUCTION MACHINE PARAMETERS

Parameters	Value	Unit
Nominal power, P_n	50.0	hp
Nominal voltage, V_n	460.0	V
Stator phase resistance, R_s	0.087	Ω
Rotor phase resistance (referred to stator), R'_r	0.228	Ω
Stator leakage inductance, L_{ls}	0.0008	H
Rotor leakage inductance (referred to stator), L'_{lr}	0.0008	H
Magnetizing inductance, L_m	0.0347	H
Number of pole pairs	2	-
Combined rotor and load moment of inertia, J_m	1.662	kg·m^2
Viscous friction coefficient, b	0.01	Nms

A speed control loop ensures that the motor's speed follows the desired reference, using a field-oriented control (FOC) strategy to optimize efficiency. The control algorithm evaluates electrical and thermal models to minimize power losses and estimate junction temperature. Virtual resistance-based power routing dynamically adjusts current distribution between the converters based on condition monitoring, ensuring thermal balancing. The reference current inputs and thermal feedback help determine the optimal switching actions. The entire system is designed to enhance reliability, reduce thermal stress, and maintain operational efficiency under varying loads and conditions.

IV. SIMULATION RESULTS

To validate the effectiveness of the proposed control framework, simulations of the motor drive system are carried out using MATLAB/Simulink software. The control strategy integrates both electrical and thermal models to optimize the electrical and thermal performance of the motor drive. The degradation rate of NPC_2 is considered to be more than the degradation rate of NPC_1 during the simulations. In the next section, the effectiveness of the developed thermal management framework is investigated under different scenarios.

Case A: Without power routing

The electrothermal performance of the system without any power routing is illustrated in Figure 7. Here, the load is shared equally between the two converters. Moreover, the junction temperature of only the first MOSFET of both converters is presented for comparison.

From Figure 7, it can be seen that the maximum junction temperatures reached are approximately 77.5°C for NPC_1 and 83.5°C for NPC_2. This difference in junction temperature is

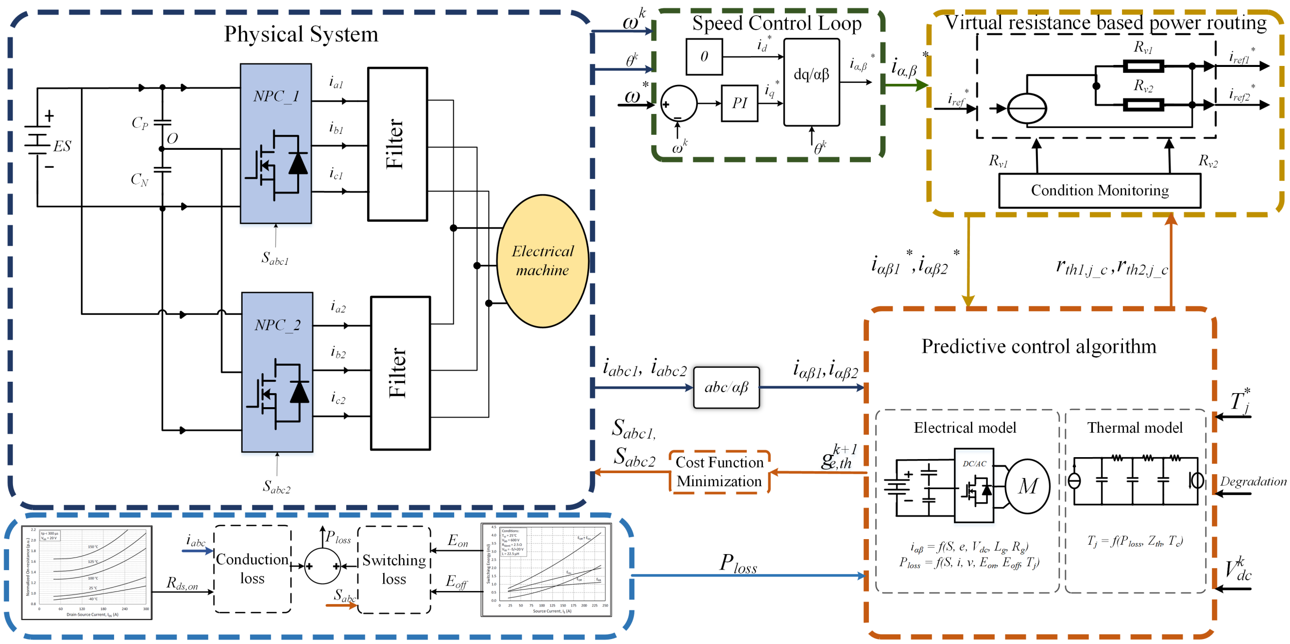

Fig. 6. Electrothermal management framework for parallel NPC converters

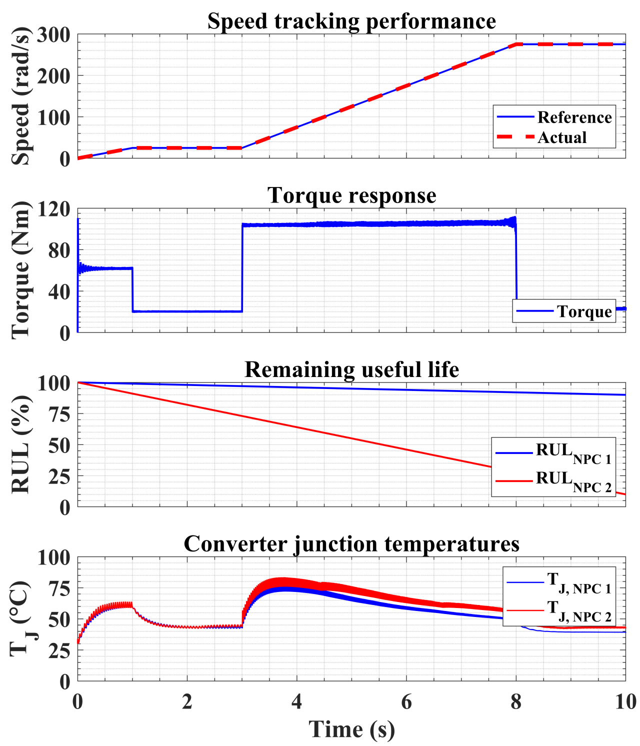

Fig. 7. Junction temperature and machine responses

due to two different degradation rates. As NPC_2 is experiencing higher junction temperature, it has a higher probability of breaking down in the future if the operating conditions remain the same. Also, in 7, the system's speed and torque responses are illustrated. The actual speed closely follows the reference speed. The electromagnetic torque also stabilizes after some initial oscillations. These results demonstrate the speed and torque tracking capability of the developed control system. Figure 8 demonstrates the thermal parameters of the MOSFETs during high speed and torque conditions.

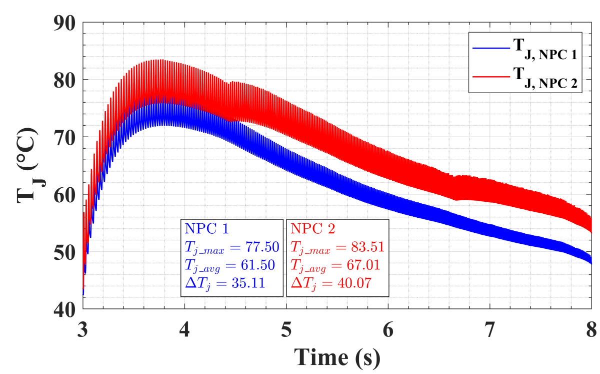

Fig. 8. Thermal performance during high torque and speed condition

Due to higher degradation, the maximum junction temperature ($T_{j,max}$), average junction temperature ($T_{j,avg}$) and thermal cycle (ΔT_j) values of NPC_2 is considerably higher than NPC_1. There is a difference of 6^0C, 5.5^0C and 4.9^0C in the $T_{j,max}$, $T_{j,avg}$ and ΔT_j values, respectively, between the two converters. These are indications that the MOSFET in NPC_2 is likely to fail early compared to NPC_1.

Case B: With power routing

Figure 9 illustrates the drive system's electrothermal performance once power routing is employed. Here, the load is shared equally between the two converters until 3s, and afterward, power routing is applied.

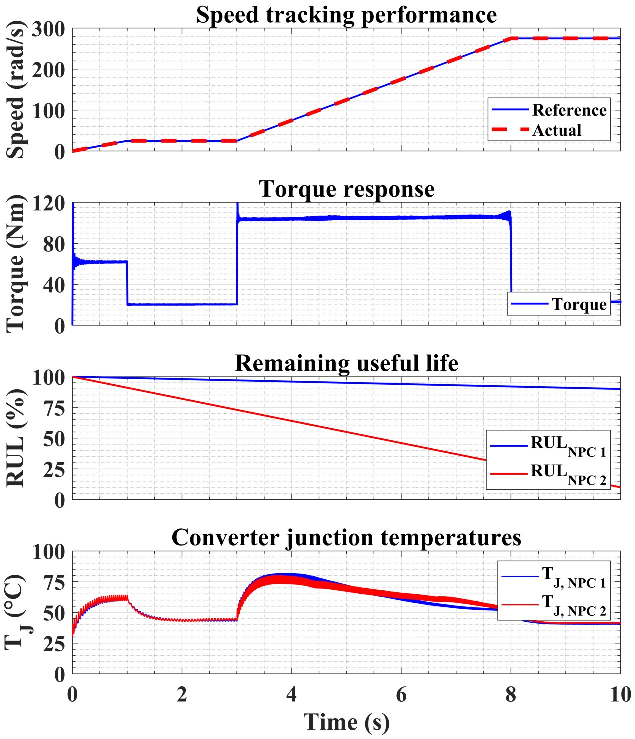

Fig. 9. Junction temperature and machine responses

From the figure, it can be observed that the maximum junction temperatures reached are approximately 82.1°C for NPC_1 and 80.4°C for NPC_2. As the power routing algorithm is applied, the load across NPC_2 is reduced, and the load across NPC_1 is increased, hence the change in maximum junction temperatures compared to $Case A$. This results in lesser thermal stress on NPC_2 and prevents it from breaking down early. The system's speed and torque responses show that even after the application of power routing, the speed and torque tracking capability of the developed control system is very accurate. Figure 10 demonstrates the thermal performance of the MOSFETs during high speed and torque conditions.

There is a difference of 1.7^0C, 0.37^0C and 2.4^0C in the $T_{j,max}$, $T_{j,avg}$ and ΔT_j values, respectively, between the two converters now. These differences are considerably lesser than $Case A$ and indicate a more uniform distribution of thermal load.

V. Conclusion

This paper proposes a power routing-based thermal management system for two parallel connected SiC-based NPC inverters driving an induction motor. The system integrates electrical control by MPC and thermal management via virtual resistance-based power routing to ensure efficient and reliable operation. To protect the more degraded converter and ensure its longevity, the system adapts by increasing the load on the less degraded converter. This is done by regulating two virtual

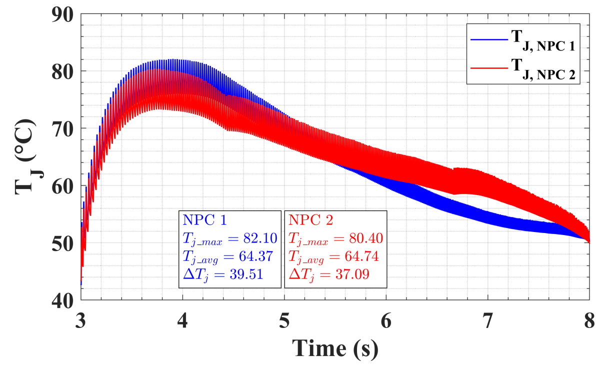

Fig. 10. Thermal performance during high torque and speed condition

resistance values (VR_1 and VR_2) which are adjusted over time to balance the thermal stress between the converters. The developed power routing method can be applied to optimize the RUL of heavily degraded converters in a multi-converter-based ship power system. The limitation of the proposed algorithm is that it can only be applied during partial loading conditions. Integrating an improved degradation model to enhance the effectiveness of this power routing-based thermal management approach and the real-time implementation of the proposed method is left for future work.

Acknowledgment

This material is based upon research supported by the US Office of Naval Research (ONR) under award number N00014-22-1-2558, and it is approved for public release under DCN# 2025-2-11-584. The authors would like to acknowledge the Warren H. Owen Distinguished Professorship Endowment for its support of the research effort.

References

[1] A. Emadi, Y. J. Lee, and K. Rajashekara, "Power electronics and motor drives in electric, hybrid electric, and plug-in hybrid electric vehicles," *IEEE Transactions on Industrial Electronics*, vol. 55, no. 6, pp. 2237–2245, 2008.

[2] S. Castellan, R. Menis, A. Tessarolo, F. Luise, and T. Mazzuca, "A review of power electronics equipment for all-electric ship mvdc power systems," *International Journal of Electrical Power & Energy Systems*, vol. 96, pp. 306–323, 2018.

[3] S. I. Rahman, M. R. Hazari, S. U. Hani, B. B. Pathik, M. A. Mannan, A. Mahfuz, M. K. Alam, and M. K. Hassan, "Primary frequency control of large-scale pv-connected multi-machine power system using battery energy storage system," *International Journal of Power Electronics and Drive Systems*, vol. 12, no. 3, p. 1862, 2021.

[4] M. Liserre, T. Sauter, and J. Y. Hung, "Future energy systems: Integrating renewable energy sources into the smart power grid through industrial electronics," *IEEE Industrial Electronics Magazine*, vol. 4, no. 1, pp. 18–37, 2010.

[5] G. Buticchi, S. Bozhko, M. Liserre, P. Wheeler, and K. Al-Haddad, "On-board microgrids for the more electric aircraft—technology review," *IEEE Transactions on Industrial Electronics*, vol. 66, no. 7, pp. 5588–5599, 2019.

[6] S. Yang, A. Bryant, P. Mawby, D. Xiang, L. Ran, and P. Tavner, "An industry-based survey of reliability in power electronic converters," *IEEE Transactions on Industry Applications*, vol. 47, no. 3, pp. 1441–1451, 2011.

[7] M. Reynell, “Advanced thermal analysis of packaged electronic systems using computational fluid dynamics techniques,” *Computer-aided engineering journal*, vol. 7, no. 4, pp. 104–106, 1990.

[8] M. Liserre, M. Andresen, L. Costa, and G. Buticchi, “Power routing in modular smart transformers: Active thermal control through uneven loading of cells,” *IEEE Industrial Electronics Magazine*, vol. 10, no. 3, pp. 43–53, 2016.

[9] G. Ozkan, P. H. Hoang, P. R. Badr, C. S. Edrington, and B. Papari, “Real-time thermal management for two-level active rectifier with finite control set model predictive control,” *International Journal of Electrical Power & Energy Systems*, vol. 131, p. 107057, 2021.

[10] S. I. Rahman, A. Moghassemi, A. Arsalan, L. Timilsina, P. K. Chamarthi, B. Papari, G. Ozkan, and C. S. Edrington, “Emerging trends and challenges in thermal management of power electronic converters: A state of the art review,” *IEEE Access*, vol. 12, pp. 50 633–50 672, 2024.

[11] M. Liserre, G. Buticchi, J. I. Leon, A. M. Alcaide, V. Raveendran, Y. Ko, M. Andresen, V. G. Monopoli, and L. Franquelo, “Power routing: A new paradigm for maintenance scheduling,” *IEEE Industrial Electronics Magazine*, vol. 14, no. 3, pp. 33–45, 2020.

[12] A. Moghassemi, G. Ozkan, C. S. Edrington, G. Muriithi, and Z. Zhang, “Active thermal control of ac/dc power converter considering health monitoring of power modules,” in *2023 IEEE Electric Ship Technologies Symposium (ESTS)*, 2023, pp. 78–85.

[13] A. Marquez, J. I. Leon, S. Vazquez, and L. G. Franquelo, “Closed-loop active thermal control via power routing of parallel dc-dc converters,” in *2018 IEEE 12th International Conference on Compatibility, Power Electronics and Power Engineering (CPE-POWERENG 2018)*, 2018, pp. 1–6.

[14] A. Marquez, J. I. Leon, S. Vazquez, L. G. Franquelo, G. Buticchi, and M. Liserre, “Power device lifetime extension of dc-dc interleaved converters via power routing,” in *IECON 2018-44th Annual Conference of the IEEE Industrial Electronics Society*, 2018, pp. 5332–5337.

[15] V. Raveendran, M. Andresen, and M. Liserre, “Improving onboard converter reliability for more electric aircraft with lifetime-based control,” *IEEE Transactions on Industrial Electronics*, vol. 66, no. 7, pp. 5787–5796, 2019.

[16] ——, “Reliability oriented control of dc/dc converters for more electric aircraft,” in *2018 IEEE 27th International Symposium on Industrial Electronics (ISIE)*, 2018, pp. 1352–1358.

[17] M. Andresen, J. Kuprat, V. Raveendran, J. Falck, and M. Liserre, “Active thermal control for delaying maintenance of power electronics converters,” *Chinese Journal of Electrical Engineering*, vol. 4, no. 3, pp. 13–20, 2018.

[18] G. Buticchi, M. Andresen, M. Wutti, and M. Liserre, “Lifetime-based power routing of a quadruple active bridge dc/dc converter,” *IEEE Transactions on Power Electronics*, vol. 32, no. 11, pp. 8892–8903, 2017.

[19] Y. Ko, M. Andresen, G. Buticchi, and M. Liserre, “Thermally compensated discontinuous modulation strategy for cascaded h-bridge converters,” *IEEE Transactions on Power Electronics*, vol. 33, no. 3, pp. 2704–2713, 2017.

[20] Y. Ko, V. Raveendran, M. Andresen, and M. Liserre, “Advanced discontinuous modulation for thermally compensated modular smart transformers,” *IEEE Transactions on Power Electronics*, vol. 35, no. 3, pp. 2445–2457, 2019.

[21] V. G. Monopoli, A. Marquez, J. I. Leon, Y. Ko, G. Buticchi, and M. Liserre, “Improved harmonic performance of cascaded h-bridge converters with thermal control,” *IEEE Transactions on Industrial Electronics*, vol. 66, no. 7, pp. 4982–4991, 2018.

[22] Y. Ko, M. Andresen, G. Buticchi, and M. Liserre, “Power routing for cascaded h-bridge converters,” *IEEE Transactions on Power Electronics*, vol. 32, no. 12, pp. 9435–9446, 2017.

[23] M. Andresen, V. Raveendran, G. Buticchi, and M. Liserre, “Lifetime-based power routing in parallel converters for smart transformer application,” *IEEE Transactions on Industrial Electronics*, vol. 65, no. 2, pp. 1675–1684, 2017.

[24] C. Barbagallo, S. A. Rizzo, G. Scelba, G. Scarcella, and M. Cacciato, “On the lifetime estimation of sic power mosfets for motor drive applications,” *Electronics*, vol. 10, no. 3, 2021.

[25] C. Sintamarean, H. Wang, F. Blaabjerg, and F. Iannuzzo, “The impact of gate-driver parameters variation and device degradation in the pv-inverter lifetime,” in *2014 IEEE Energy Conversion Congress and Exposition (ECCE)*, 2014, pp. 2257–2264.

[26] J. Rodriguez, S. Bernet, P. K. Steimer, and I. E. Lizama, “A survey on neutral-point-clamped inverters,” *IEEE Transactions on Industrial Electronics*, vol. 57, no. 7, pp. 2219–2230, 2010.

[27] S. I. Rahman, G. Ozkan, A. Arsalan, P. K. Chamarthi, B. Papari, and C. S. Edrington, “Impact of active cooling on the thermal management of 3-level neutral point clamped (npc) converter for hybrid electric vehicle application,” SAE Technical Paper, Tech. Rep., 2023.